Tribology Letters (2023) 71:127
https://doi.org/10.1007/s11249-023-01799-0

ORIGINAL PAPER

Tribo-Electric Analysis of Multi-Cycle Wear in Asymmetric Laser-Structured Cu-Sn Connectors

Silas Schütz[1,2] · **Sebastian Suarez**[1,2] · **Frank Mücklich**[1,2,3]

Received: 8 September 2023 / Accepted: 19 October 2023 / Published online: 14 November 2023

Abstract
One of the key objectives of the connector industry for the past years has been to reduce the insertion friction forces of detachable electrical connections, where the majority of approaches combine a particular connector design with the usage of lubricants. The necessity for a solution that uses less contact force to maintain a lasting electrically conductive connection without sacrificing the mechanical robustness of the connection during use is a significant challenge in this situation. The approach in this work is to create surfaces supporting asymmetric friction, meaning lower insertion than removal forces. By Direct Laser Interference Patterning (DLIP), asymmetric saw-tooth structures with different structural inclinations and periodicities were generated on Sn-coated Cu plates. It is determined that topographical interlocking is the primary operating mechanism providing the required anisotropy. Multiple insertion/removal cycles were simulated on the tailored surfaces to tribologically characterize them and to determine the evolution of the electrical contact resistance at the end of each insertion motion. The vast majority of the generated structures showed an improvement compared to the reference state, with lower insertion and higher removal forces while the electrical behavior is not significantly impacted.

Keywords Friction asymmetry · Laser structuring · Cu-Sn · Connectors

1 Introduction

Friction anisotropy, the phenomenon of generating motion in a favored direction facilitated by the asymmetrical nature of a surface, is a prevalent characteristic observed in many biological systems. In their study, Ma et al. [1] investigated the friction anisotropy present in wheat awns, which exhibit a high degree of this characteristic due to the presence of oriented thorns on their surface. Inspired by these findings, 3D printed polymer structures with similar surfaces were fabricated and subjected to further investigation to determine the underlying stick–slip mechanism. Hazel et al. [2] also explored the role of friction anisotropy in biological systems, examining skin samples from three different snake species and observing the presence of fibers with asymmetrically shaped ends, leading to low friction in one direction and higher friction in the opposite direction, contributing to the snakes' locomotion mechanism. In other report, Tramsen et al. [3] fabricated different anisotropic structures, drawing inspiration from biological systems, and conducted investigations on the effects of feature size, aspect ratio, material stiffness, and roughness of non-structured counter-bodies during unlubricated sliding. The authors emphasized the intricate nature of friction behavior, which is influenced by the aforementioned factors and their interplay.

By drawing inspiration from these natural strategies, it is possible to develop approaches to create friction anisotropy in technical systems via inclined structures. The use of these structures is based on the concept of directional force decomposition. Figure 1 provides a schematic representation of the insertion and removal processes in a sliding system, with the movement direction indicated by dotted-line arrows. The solid-line arrows depict the normal forces exerted onto the structural maxima, which are related to the insertion and normal forces through the flank inclination angle. As the inclination angles decrease, the structural asymmetry increases, leading to an expected increase in the disparity

✉ Silas Schütz
silas.schuetz@uni-saarland.de

[1] Chair of Functional Materials, Saarland University, Saarbrücken, Germany

[2] Material Engineering Center Saarland, Saarbrücken, Germany

[3] SurFunction GmbH, Saarbrücken, Germany

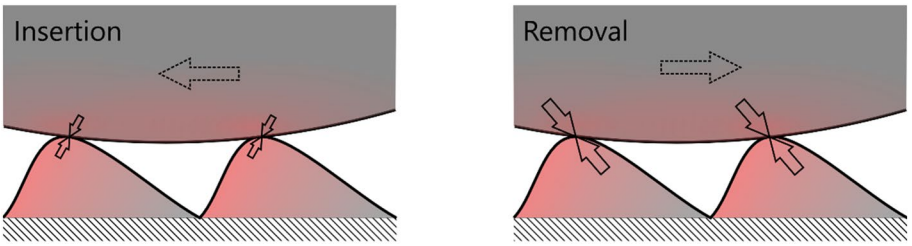

Fig. 1 Schematic representation of the forces indicated by solid-line arrows on the maxima of inclined structures during the insertion and removal processes. The dotted-line arrows depict the direction of movement

between the forces during insertion and removal. This hypothesis is in good agreement with the findings reported in [4] for single-cycle dry sliding.

An application field that would benefit from this is electrical connectivity in automotive systems, where low friction during insertion and higher friction at the operational position to prevent disconnection are required. This has been highlighted in a technical report by the German Electrical and Electronic Manufacturers' Association, which addressed the failure causes of electrical connectors in automotive onboard power supply components [5]. There, the disconnection of connectors is underlined as the most critical systematic reason for failure, causing 50% of total failures with increasing tendency during the first 3 years of operation to almost 60%.

On the other hand, low friction during insertion decreases the force needed for contacting, so that more connections for the same socket are possible without raising the overall force needed. This is a very useful feature, considering the further electrification and the increasing complexity of the electronic systems in passenger cars. Common approaches for these two issues are mechanical locking of the housing to prevent unwanted disconnection or lubricants for lower insertion forces [6]. However, a surface structure creating friction anisotropy could address both problems at once.

Notably, the role of roughness is of particular importance in connector applications due to its inherent variability in technical materials, requiring consideration during practical implementation. Additionally, the commonly employed Cu-Sn material combination gives rise to the formation of intermetallic phases (IMP), characterized by a stiffness approximately 3 times greater than that of Sn (Young's modulus: Sn: 46.9 GPa, Cu_6Sn_5: 112.3 GPa, Cu_3Sn: 134.2 GPa) [7]. Considering the wear of Sn during the connector's lifespan, it becomes possible for the intermetallic compound to emerge at the surface and influence both the tribological and electrical behavior. This aspect also requires careful consideration in the design of the system.

Direct Laser Interference Pattering (DLIP) is a suitable technology to apply periodic structures to surfaces of a wide variety of materials [8–10]. Their influence on the tribological behavior has been broadly investigated in recent times, where a reduction of the coefficient of friction (COF) was frequently observed [11–13]. The surface structures reduce the real contact area, due to outstanding asperities which predominantly contact the counter-body and since [14] the friction force is directly proportional to the real contact area (as defined by Bowden and Tabor [14]), this derives into a reduction of the friction force. However, the friction force is reduced in both directions since it is a symmetric effect. To create an asymmetrical effect, the surface pattern needs to be asymmetric. Voisiat et al. [15] created saw-tooth-like surface on stainless steel by tilting the sample and structuring it using DLIP, whereas Alamri et al. [16] used a similar setup to structure polymer foils, obtaining well defined periodic structures.

In a previous study [4], this methodology was employed to generate inclined laser structures on Sn-coated Cu plates, which was already mentioned, are widely used as connector materials. By using a rotational stage, the samples were tilted at predetermined angles (i.e., 15°, 30°, and 45°), followed by irradiation with a picosecond pulsed laser beam. The varying tilt angles resulted in the formation of asymmetric flanks in the inclined structures. Subsequently, these structures were thoroughly characterized, and their tribo-electrical behavior was investigated to analyze their performance during the initial insertion and removal cycles. The findings revealed that most of the samples exhibited the predicted asymmetric behavior, with a lower coefficient of friction (COF) observed during insertion compared to removal. Particularly, the 15° inclination regularly outperformed the reference state and demonstrated the most favorable overall performance considering the parameters examined. This is associated to the fact that a 15° inclination results in steeper flanks that favor interlocking between the contacting bodies. However, it is important to note that only the first insertion and removal cycles were studied in this investigation.

In this study, we present an approach aimed at elucidating the impact of asymmetric structures on friction phenomena for multi-cycle testing. To gain a more comprehensive understanding of these mechanisms over an extended duration, we reproduce similar structures as described in the previous study [4] and investigate the tribological and electrical behavior at the interface across a larger number of insertion/removal cycles.

2 Materials and Methods

2.1 Test Specimens

Hot-dipped tinned Cu platelets, as-received and aged, were investigated (Fig. 2a and b, respectively). No specific protocol was followed to achieve ageing. The material was stored under ambient conditions for approximately two years without any heat treatment. The main difference between both sample types is the fraction of intermetallic phases (IMP) formed. The IMP closer to the substrate is Cu_3Sn (ε) and the one closer to the Sn topcoat is Cu_6Sn_5 (η). These phases are formed immediately after the deposition process and grow due to aging [17]. In Table 1, the resistivities of the pure metals and the IMPs are given. In the as-received state, the Sn top layer has a thickness between 1.5 µm and 4.1 µm, whereas in the aged state, the IMP growth results in 0.5 µm Sn in the uppermost layer. The total thickness (Sn + IMP) was in all cases (3 ± 2) µm. The plates were obtained from stripes that were cut into (15×30) mm^2 pieces and cleaned in an ultrasonic bath with acetone and isopropanol for 5 min in each solvent.

Table 1 Resistivities of the pure metals and the IMPs

Material	Resistivity $/10^{-8}\Omega \cdot m$
Cu	1.68 [18]
Sn	11.5 [18]
Cu_3Sn	8.80 [19]
Cu_6Sn_5	1.75 [19]

2.2 Surface Structuring of the Specimens

Direct Laser Interference Patterning (DLIP) was chosen as the structuring method for the generation of the inclined structures. DLIP creates a periodic intensity pattern by splitting a linear polarized laser beam into two sub-beams and interfering them onto the sample's surface. Constructive interference leads to maxima and minima are formed by destructive interference. The pattern's periodicity is calculated following $\Lambda = (\lambda/2) \bullet \sin(\theta)$. Where Λ is the structural periodicity, λ is the laser wavelength and θ the half-angle between the interfering beams. The principle is illustrated schematically in Fig. 3. The literature provides a more detailed description of the process [20–22].

This study uses an RDX 500 Nano picolaser system (Pulsar Photonics, Germany), which combines an optical head from the Fraunhofer IWS with an Edgewave InnoSlab PX

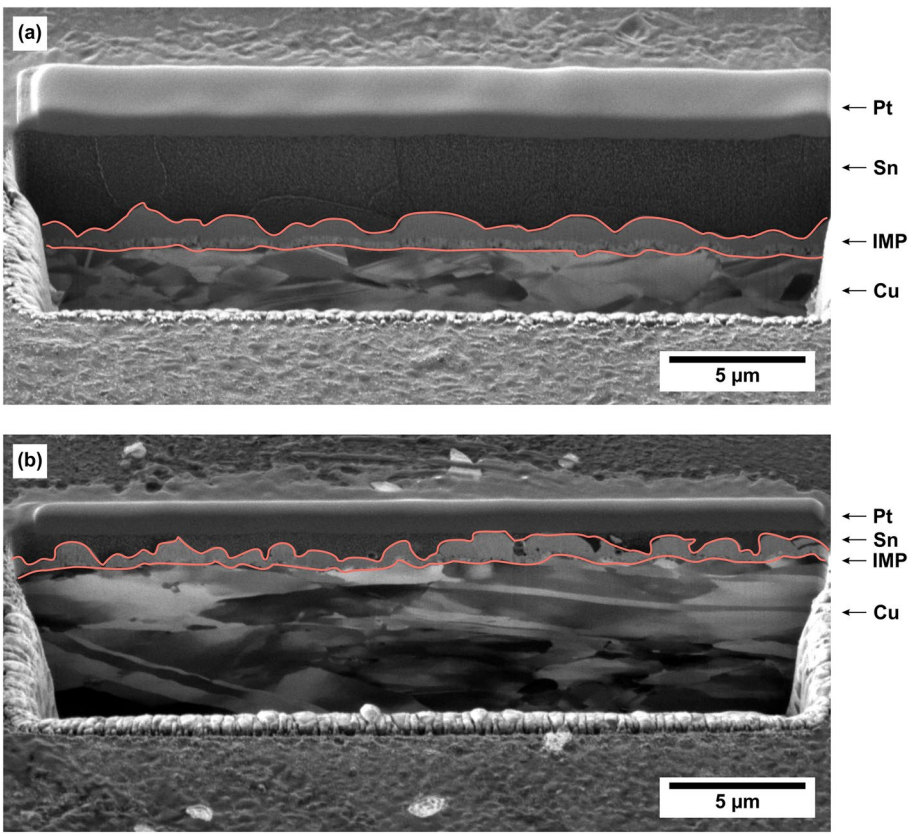

Fig. 2 Sn-coated plates in cross section, shown as received (**a**) and aged (**b**). There are indications of the various constituent phases. Both cross sections have a Pt layer placed on top to shield the original surface

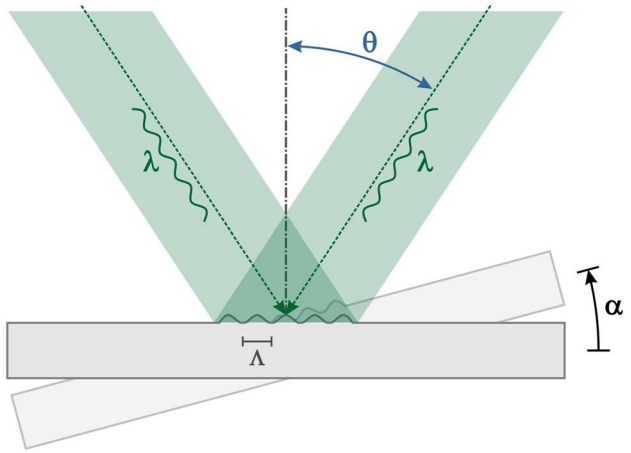

Fig. 3 Principle of DLIP and setup for inclined surface structures presented schematically

laser with a pulse length of 12 ps and 532 nm wavelength. Here, a line-like pattern is produced via two-beam laser interference. The optical head has all the optics required to divide the main laser beam and vary the angle at which the split beams are focused. Samples having symmetrical line-like structures ($\alpha = 0°$) with periodicities of 5 µm, 7.5 µm, and 10 µm were produced. To generate asymmetry, the sample is tilted by a defined angle α, as schematically shown in Fig. 3. Asymmetrical saw-tooth shaped structures with the aforementioned periodicities and different tilt angels ($\alpha = 15°, 30°, 45°$) were created. In addition to the patterned samples unmodified references were studied. In total, 26 different sample types were examined. Prior to further analysis, all samples were cleansed once again in isopropyl alcohol in an ultrasonic bath for 10 min.

2.3 Surface Characterization

The structures created by DLIP and the reference samples were analyzed using confocal laser scanning microscopy (CLSM, Olympus OLS 4100) and scanning electron microscopy (SEM, FEI Helios NanoLab600) in combination with focused ion beam microscopy (FIB). CLSM data was collected using a 405 nm laser and a 50 × objective (N.A. = 0.95) with a resolution of 10 nm in the Z direction and 120 nm in the X–Y directions. A profile line was exported from each measurement, which are shown in extracts in Fig. 4. Additionally, roughness parameters are given in Table S1 and S2. The sides of the topographical maxima have a distinct inclination that distinguishes them from typical DLIP-obtained structures (0°). There are no discernible variations between the as-received and aged materials from a strictly topographical standpoint. This can also be seen in the roughness parameters.

The SEM pictures were acquired with a secondary electron detector with 5 and 10 keV.

2.4 Tribo-Electrical Characterization

A custom-built multipurpose test device, as outlined in reference [23], was used to imitate insertion and removal movements. The test device consists of a two-axis translational stage and a force sensor. The sample is mounted on the force sensor and the counter-body is brought into contact

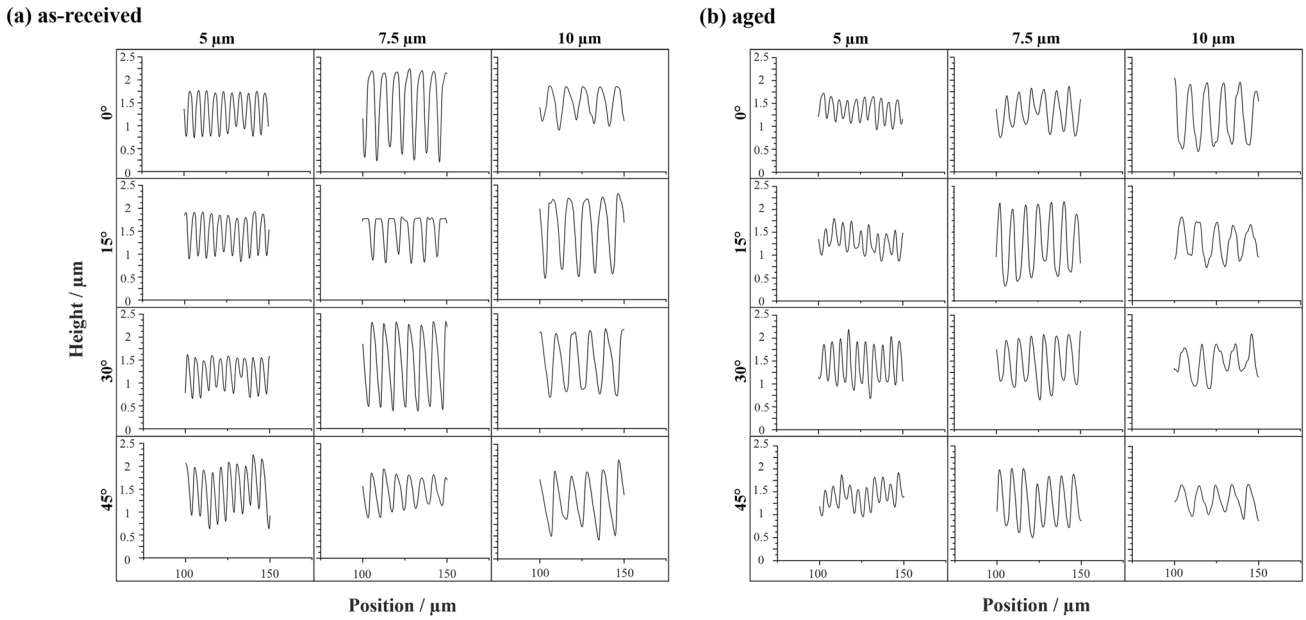

Fig. 4 Profile lines from confocal laser scanning images of all structured samples

and moved over the sample via the linear stages. For the purpose of tribo-electrical characterization, spherical pure Cu rivets (head diameter: 5.4 mm, curvature radius: 3 mm) were selected as the counter-bodies. These round rivets, with a root mean square roughness (Sq) of 0.595 µm, were utilized in their as-received state, except for a 10-min cleaning in an ultrasonic bath with isopropanol to remove any superficial contaminant films. Functioning as the cathode, the rivets were brought into contact with the sample, which served as the anode. Additionally, an unstructured reference sample was also tested for benchmarking.

In the course of a measurement cycle, the sample was subjected to contact with a rivet, resulting in a surface scratch spanning a distance of 3 mm. The scratch was produced by the rivet moving at a velocity of 15 mm/s, aiming to replicate an insertion scenario. Throughout this process, a constant normal load of 1 N was applied. To assess the electrical contact resistance (ECR) under dry circuit conditions ($I_{DC} = 100$ mA), five measurements were conducted using the four-wire method with a current source (2400 SMU) and a nanovoltmeter (2182A) by Keithley. The results of these measurements were averaged for each cycle. Subsequently, the rivet was moved in the opposite direction to simulate the removal process. The coefficient of friction (COF) was continuously monitored during each motion. 20 cycles were tested per sample following the standard quality assurance test used in the automotive industry [6, 24].

3 Results and Discussion

3.1 Wear Track Morphological Characterization

Analogous to the characterization of the structures prior to the measurements, the reversal points of the tested wear tracks were analyzed by confocal laser scanning microscopy. Light microscopy images were acquired from each measurement, which are shown in Fig. 5. According to the technical guide TLF 0214 by the German Electrical and Electronic Manufacturers' Association a light microscopic inspection provides valuable information as a final examination after conducting tribo-electrical tests [25]. For the as-received material, depicted in Fig. 5a, no structures could have been identified after 20 measurement cycles. However, the base material is not yet exposed on the surface. This can be concluded from the fact that no copper-colored material can be identified. All tracks present significant material pile ups at the reversal point, evidencing severe plastic deformation (ploughing) of the structures (Figures S1 and S2). Furthermore, from the profiles shown in the supplementary info, there are indications that the structures might have been filled with plastically displaced material, since the height level of the interior of the track is—in several cases—above the level of the original structures.

In Fig. 5b, the measurement tracks on aged material are depicted. Here, the initial topographies can be identified in some cases (e.g., 7.5 µm with 30° and 45° inclination), although the damage is widespread. Due to an initial smaller amount of residual Sn, the IMPs have a larger significance in the structures' mechanical behavior. This can also be identified by the reddish coloring of the surfaces. The IMPs are approximately 30 × harder than pure Sn (i.e., Sn: 0.22 GPa, Cu_6Sn_5: 6.38 GPa, Cu_3Sn: 6.12 GPa) [7], which results in more mechanically stable structures. The copper-colored pile-ups, particularly noticeable on 10 µm/0° for example, might originate from the copper rivets used as counter-bodies due to material transfer, since the hardness of the Cu rivet is 1.38 GPa. This poses a challenge to the interpretation, since it is not trivial to assess the origin of the material in the pile ups by traditional methods (e.g., EDS). With a certain degree of certainty, it can be stated that the base material has not been exposed on the surface here, as in the as-received state.

3.2 Friction Characteristics of the As-received and Aged Materials

To evaluate the effect of asymmetric structuring in a more straightforward way, a ratio relating the COF value of the structured surface and the flat reference is calculated, namely the evaluation parameter $\Psi = COF^{structured}/COF^{reference}$. Since in both cases the applied normal load is the same, this ratio also represents the ratio of the insertion forces in both cases, the structured and benchmark surfaces. The objective is to improve the characteristics of the tribological systems by reducing the insertion force and increasing the removal force, hence adjusting the system's performance to the requirements mentioned in the introduction of this contribution. Specifically, $\Psi_{insertion}$ should be lower than 1, and $\Psi_{removal}$ should have a value larger than 1. From here onwards, only cycles number 1, 5, 10, 15 and 20 of each measurement are shown in the figures for better clarity, along with their corresponding standard deviation.

Figure 6a presents the insertion ($\Psi_{insertion}$) friction results for the as-received state. A clear trend is visible for all periodicities, where the value predominantly starts above 1 with two exceptions (5 µm/0° and 10 µm/15°) scattered over a relatively large range (high initial friction), rapidly declining during the first cycles and converging to values marginally below the threshold after 20 cycles. This convergence is a consequence of the flattening of the surface features, homogenizing the contact area for all configurations. This is especially marked in the as-received state, since soft Sn comprises the majority of the contact interface. Notably, after 20 cycles the COF for insertion is in all cases lower than that

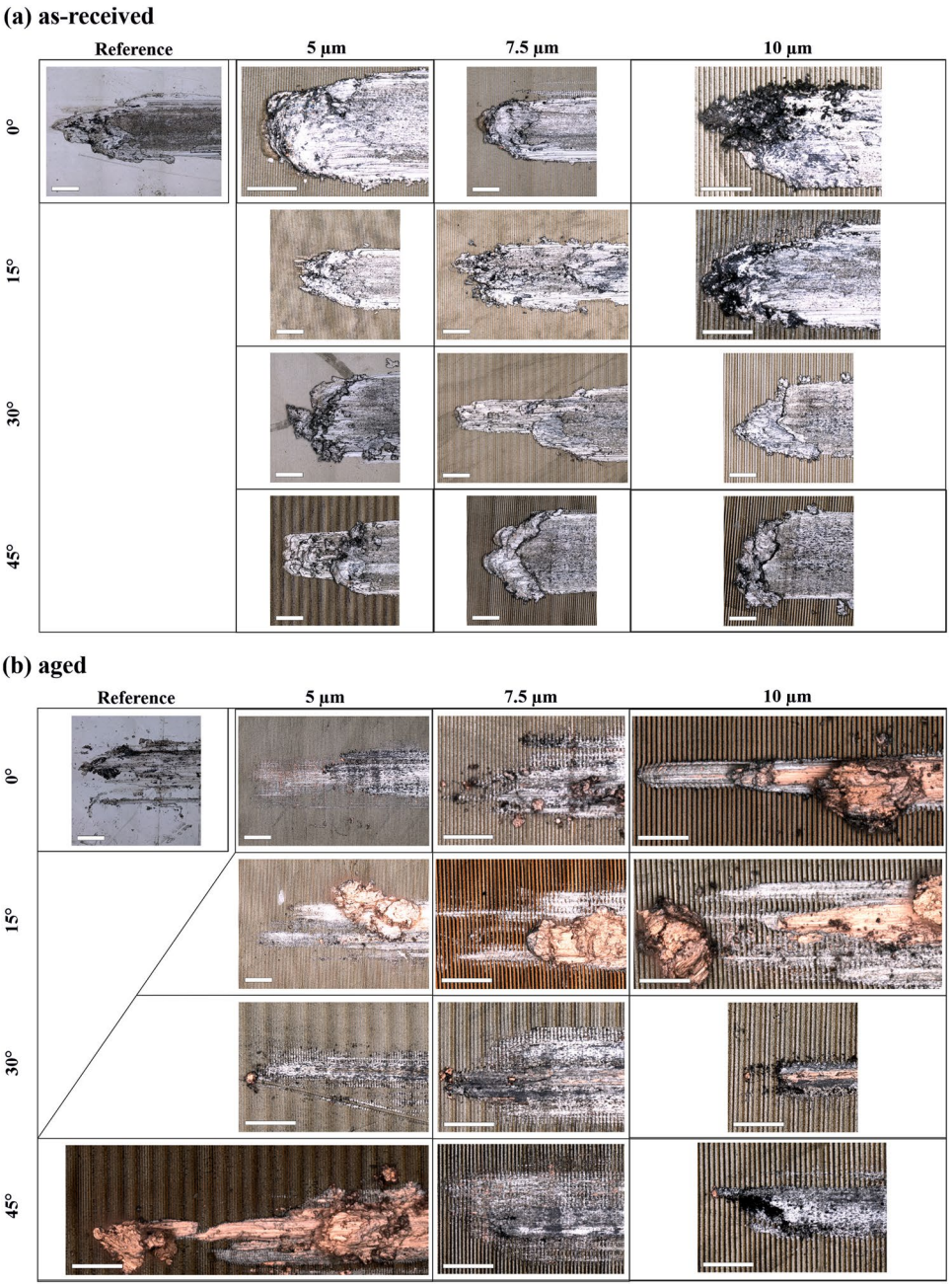

Fig. 5 Light microscopy images of the reversal point of the wear tracks of all structured samples and a reference. The scale bar represents 100 µm

of the reference for the structured samples, which was the intended aim. In general, the real contact area increases with increasing number of cycles due to plastic deformation. The patterns retard this increase leading to smaller contact areas and smaller insertion forces for the structured samples than for the reference after the same number of cycles.

For Ψ_{removal}, displayed in Fig. 6b, a similar trend is visible: the value mostly starts above or at 1 with a few exceptions, including the ones mentioned before (5 µm/0°, 5 µm/15° and 10 µm/15°), has a minimum lower than 1 around cycle 10 and increases again, being greater than 1 after 20 cycles in all cases. Thus, the COF for removal is in all cases greater for the structured samples than for the reference. Considering this and $\Psi_{\text{insertion}}$ being lower than 1, the asymmetric structures seem to facilitate the desired friction anisotropy on the as-received material compared to the reference. Even the symmetric structures without inclination show a lower COF than the reference during insertion and a higher one during removal. Given that the as-received material has significant amount of residual Sn, the dominant wear mechanism is expected to be plastic deformation of the structures, leading to an asymmetric shape after insertion, impeding the removal.

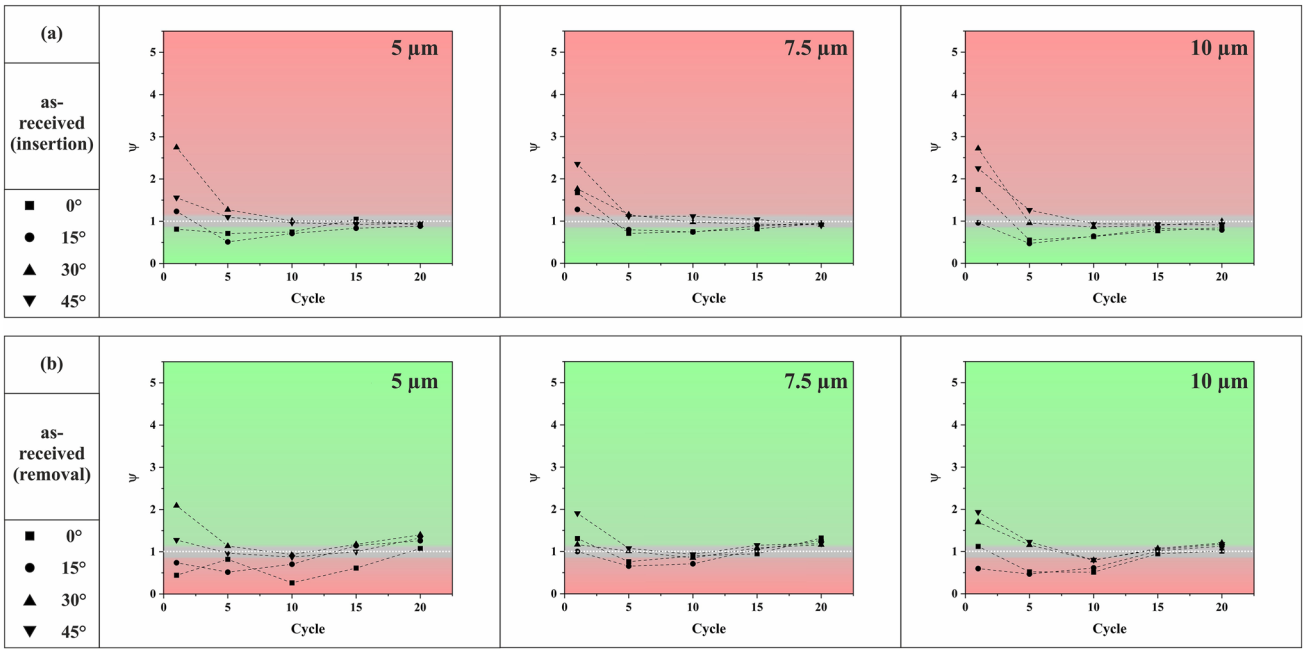

Fig. 6 **a** $\Psi_{insertion}$ for the measurements on as-received material with structured surface. **b** $\Psi_{removal}$ for the measurements on as-received material with structured surface

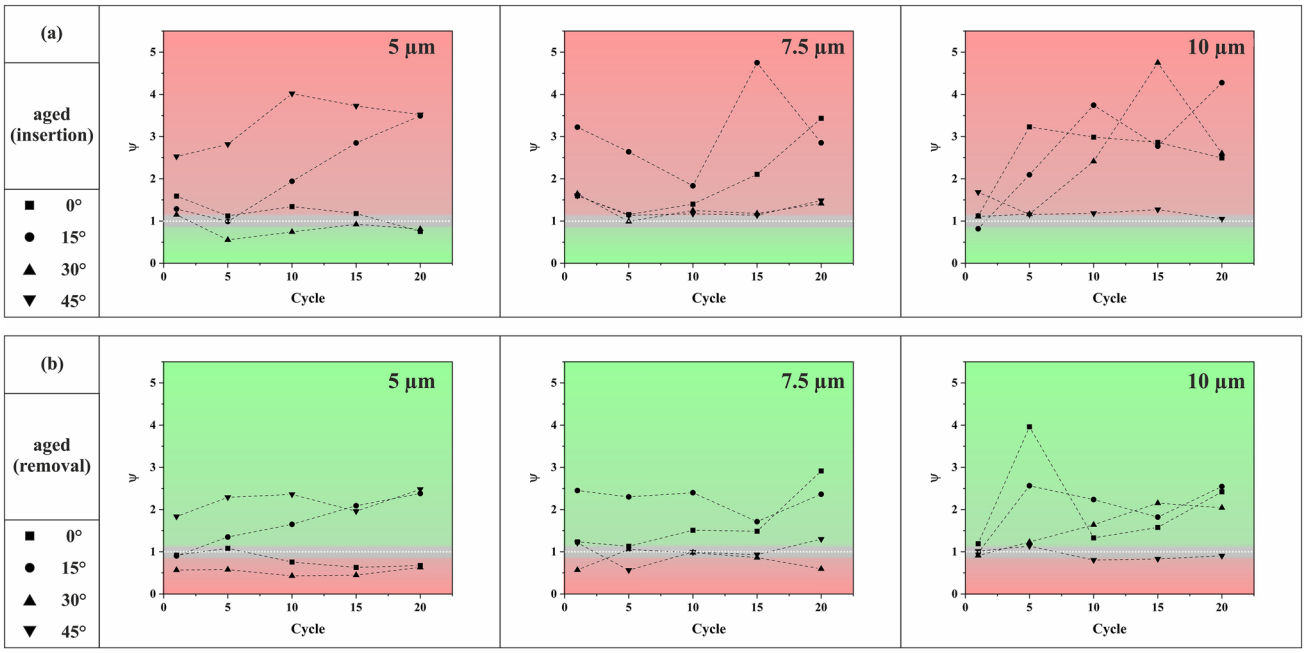

Fig. 7 **a** $\Psi_{insertion}$ for the measurements on aged material with structured surface. **b** $\Psi_{removal}$ for the measurements on aged material with structured surface

In Fig. 7a, the ratio $\Psi_{insertion}$ for the aged material is shown. No clear trend can be seen, but apart from the values for the structures with 5 µm periodicity and 30° inclination, most are greater than 1 during the whole measurement, meaning the COF of the structured samples is higher than for the reference. The largest difference between reference and structure after 20 cycles was measured for 10 µm periodicity and 15° inclination. In contrast to the as-received material, the performance of the samples with

15° inclination are in the lower range and the 5 µm/30° structure is the only one showing the desired effect.

Similar observations can be made for $\Psi_{removal}$, displayed in Fig. 7b. However, a value above 1 is envisaged and most structures fulfil this, having a higher COF during removal than the reference. Exceptions are the structures with 5 µm periodicity and 0° and 30° inclination, 7.5 µm and 30° inclination and 10 µm and 45° inclination, where $\Psi_{removal} < 1$, at least after 20 cycles. Only 15° inclination shows ratios above 1 for all periodicities. As described for the as-received material, an inclination of 15° generates steeper structures with higher anisotropy which leads to stronger mechanical interlocking during insertion. Although the counter-body is not structured the asperities of the Cu ball would interact with the structured plate by interlocking, considering that the roughness is in the range of the structural depth of the laser structures. In comparison to the reference, this leads to a higher COF during removal.

3.3 Friction Asymmetry Analysis

As proposed in [4], a friction asymmetry coefficient $\zeta = COF_{removal}/COF_{insertion}$ is defined and calculated. For ζ, the goal is to achieve a value above 1. This depicts higher forces during removal than during insertion, as described by Ma et al. [1].

In Fig. 8a, the ζ values for the as-received material are shown. The reference shows a clear decrease from a ζ value of approximately 1.5 to less than 0.8, being the lowest value after 20 cycles. The 15° inclination is the only one with $\zeta > 1$ after 20 cycles for all periodicities. For lower cycle numbers, most of these structures have ζ ratios above 1 as well, while the others tend to be smaller. So, only certain structures show an absolute anisotropy after 20 cycles, namely 5 µm with 30° and 45° inclination, 7.5 µm without inclination and all periodicities with 15° inclination, the latter already shown in [4] for single-cycle measurements. As described there, an inclination of 15° generates steeper structures, whereas larger angles generate more moderate flank inclinations which lead to a higher anisotropy for smaller inclination angles. A higher anisotropy of the structures leads to a higher anisotropy in friction, as shown by Tramsen et al. [3], where friction anisotropy is linked to mechanical interlocking of asperities of asymmetric sawtooth-like structures.

In Fig. 8b, the ratios for the aged material are presented. Here as well, no clear trend is visible. After 20 cycles, for the reference and all periodicities without inclination $\zeta \geq 1$ is valid. Some other samples reveal this behavior as well, namely the samples with 5 µm periodicity and 30° inclination, 7.5 µm periodicity and 15° and 45° inclination and with 10 µm periodicity and 30° and 45° inclination. It can be seen that the 5 µm/30° structure shows the requested anisotropy, although the COF for removal is lower than for the reference ($\Psi_{removal} < 1$). In the aged state, there is a lower amount of residual Sn on the surface. Therefore, the considerably stiffer intermetallic phase Cu_6Sn_5 is exposed in some areas. The fluctuations in ζ ratios, and in Ψ values as well, can be

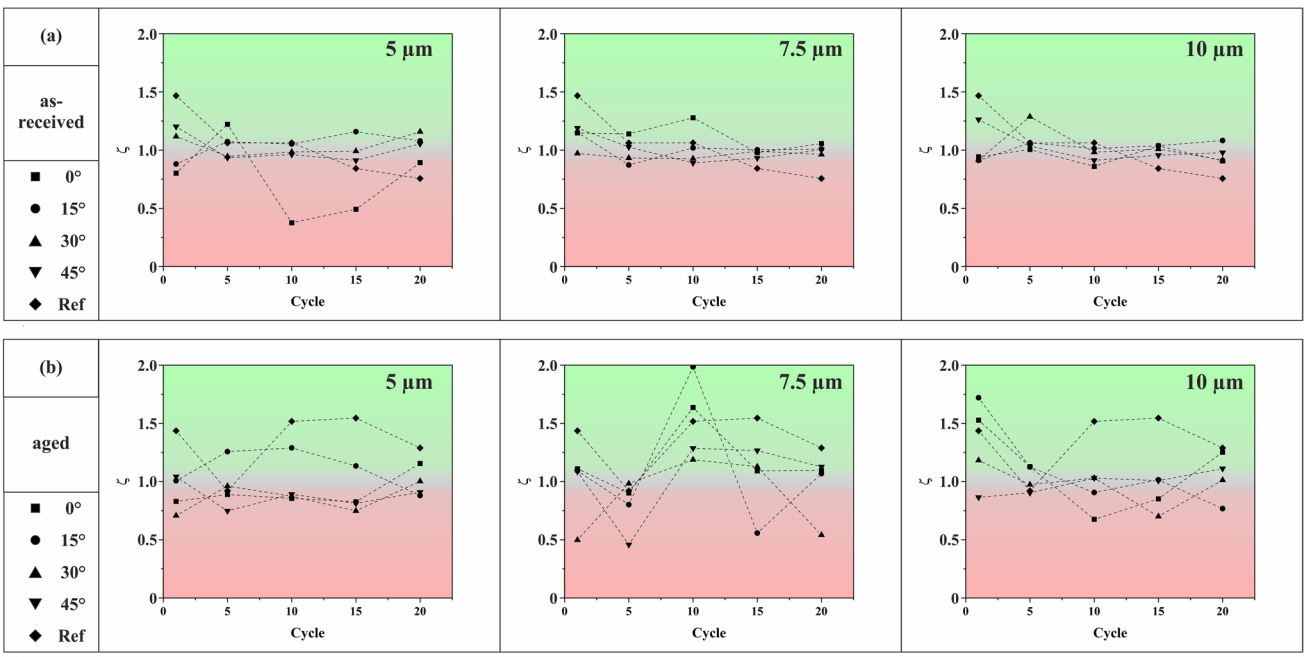

Fig. 8 **a** ζ for the measurements on as-received material with structured surface. **b** ζ for the measurements on aged material with structured surface

caused by these variations in material on the surface in the contact area.

The results of the complete tribological evaluation are schematically summarized in Table 2 for a better overview of the performances. Concerning the reduction of insertion and increase of removal forces relative to the reference, it was found that all structures on as-received material behave as intended. On the other hand, no structure on aged material shows both, with the 5 µm/30° structure being the only one with a reduction in insertion forces. Absolute anisotropy, meaning higher removal than insertion forces, is displayed by several structures, but only for 5 µm/30°, 7.5 µm /0°, 7.5 µm /15° for both materials. This summary highlights the feasibility of using this approach for the intended application.

3.4 Electrical Contact Resistance After Insertion

The presented data reflects the contact resistance in the inserted state (load still applied). In Fig. 9, the horizontal

Table 2 Summary of the results of the tribological characterization for both material types

		as-received			aged		
		$\Psi_{insertion} < 1$	$\Psi_{removal} > 1$	$\zeta > 1$	$\Psi_{insertion} < 1$	$\Psi_{removal} > 1$	$\zeta > 1$
0 µm	0°						✓
5 µm	0°	✓	✓				✓
	15°	✓	✓	✓		✓	
	30°	✓	✓	✓	✓		✓
	45°	✓	✓	✓		✓	
7.5 µm	0°	✓	✓	✓		✓	✓
	15°	✓	✓	✓		✓	✓
	30°	✓	✓				
	45°	✓	✓			✓	✓
10 µm	0°	✓	✓			✓	✓
	15°	✓	✓	✓		✓	
	30°	✓	✓			✓	✓
	45°	✓	✓				✓

The ratios after 20 cycles are considered

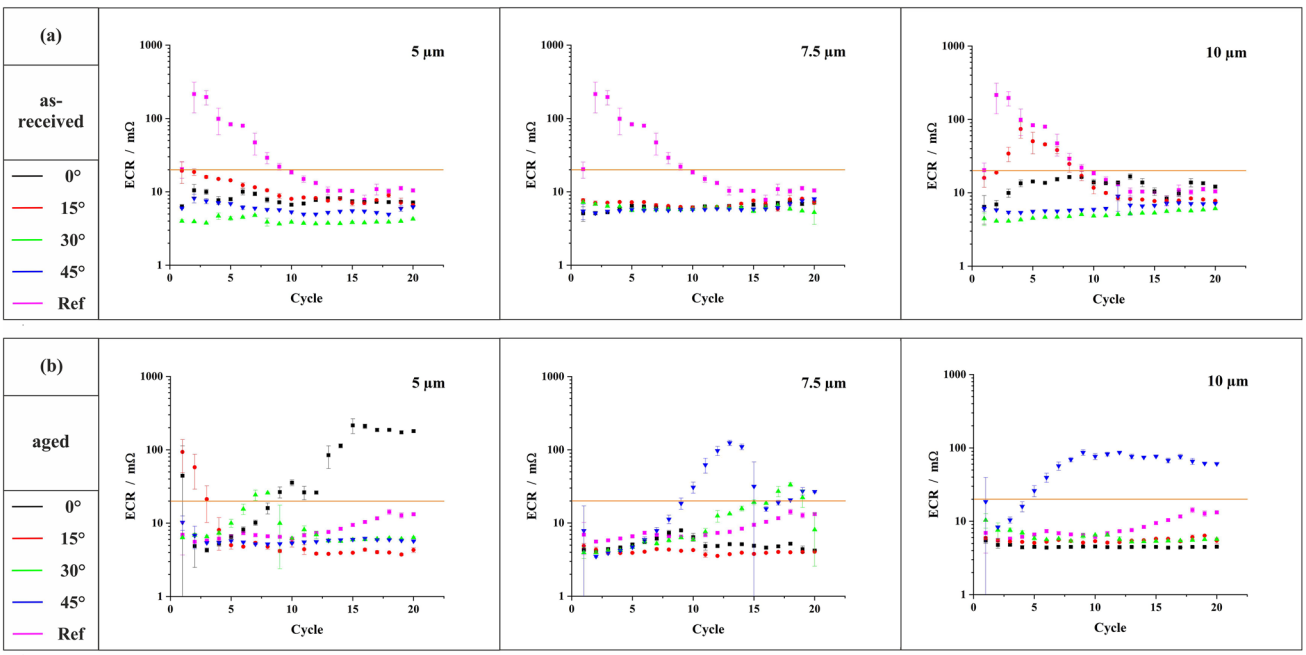

Fig. 9 ECR development for the measurements on the as-received material (**a**) and the aged material (**b**) with structured surface

line marks the threshold of 20 mΩ as recommended in literature [6].

In Fig. 9a, the ECR values for the as-received material are shown. For the reference measurement, a clear drop of the ECR from initially over 100 mΩ to around 10 mΩ from the 15th cycles onwards can be seen. It is worth remembering that in its simplest form, Holm defined ECR as the ratio of the specific electrical resistivity to the contact diameter [26]. Hence, the drop can be associated to an increase in the real contact area, the contacting against the IMPs—which have better conductivity, as stated in the Sect. 2.1—or a combination thereof. This becomes evident from the LSM optical evaluation (Fig. 5), where the Sn pile-up at the reversal point is significant, enhancing the real contact area and consequently, reducing ECR. Most of the measurements on structured samples show a more constant behavior, with ECR values around 10 mΩ. Only the measurement on the sample with 10 µm periodicity and 15° inclination shows a peak around cycle number 5, which rises to just below 100 mΩ. For all measurements, the ECR is lower than 20 mΩ after 20 cycles. In brief, the different structures do not affect the behavior after 20 cycles but the progression until 20 cycles, with the 7.5 µm periodicity performing best (almost all values are below 10 mΩ) for all inclinations.

The ECR values for the aged samples are presented in Fig. 9b. Here, the reference measurement remains fairly constant at around 10 mΩ, slightly increasing towards the 20th cycle. In comparison to the as-received material, the values belonging to the structured samples are more scattered. These fluctuations might be caused by the variations in phase distribution throughout the surface in the contact area due to less residual Sn, as described before. Another possible explanation could be supported by differences in microroughness in the contact area. After 20 cycles, all structures show an ECR below 20 mΩ, except the 5 µm periodicity without inclination and the 7.5 µm and 10 µm periodicities with 45° inclination, whereby the value belonging to the 7.5 µm/45° sample is only slightly above the recommended limit. In general, all measurements taken from aged samples lay within the same range as those from the reference condition, indicating that the patterning had no significant impact on the electrical contact resistance.

4 Conclusions

In order to determine their suitability as connection systems with friction anisotropy, saw-tooth shaped line-like DLIP structures were made on tinned Cu platelets. After characterization, they were tribo-electrically evaluated. Increased removal forces were sought after in order to stabilize connector performance and additionally reduced insertion forces in order to facilitate mounting.

The chosen patterning routine is extremely accurate and repeatable, producing the intended topography, regardless of the materials' microstructure (residual tin or IMP on the surface). Additionally, this is simply accomplished without altering the technical roughness of the plate as received. In the connection simulation, the electrical contact resistance was ascertained at the turning point and the coefficient of friction was determined during the insertion and removal movement. The values taken by three comparison ratios demonstrate that the majority of the setups under study had the predicted asymmetric behavior. For as-received material, 15° is the inclination where all periodicities show the desired behavior in all three parameters, so lower insertion and higher removal forces than the reference and lower insertion than removal forces for the sample itself. This can be explained by the fact that this inclination produces the steepest flanks [4], which are favorable to the intended interlocking mechanism. For the aged material no structure performs well in all parameters, though several in at least two.

Concerning the electrical contact resistance after insertion, the structures have little to no serious impact. It is particularly important to note that they do not deteriorate the electrical behavior. Most of the time, the ECR was below 20 mΩ, an industrial threshold. In the case of the as-received material, the structures lead to a more constant progression over the 20 measurement cycles, but do not affect the value after the last insertion, being below 20 mΩ for all structures. In the aged state, there is a lower amount of residual tin on the surface. Therefore, in some areas the Cu_6Sn_5 intermetallic phase is exposed. These fluctuations in material in the contact zone led to a more scattered progression over the 20 cycles, compared to the samples on as-received material. The broader variation relative to the reference can be explained by the laser structure, partly removing the residual Sn, and enhancing the material fluctuations. After 20 cycles the ECR is below 20 mΩ for nearly all structures on aged material as well.

Altogether, it can be concluded that asymmetric structures may be easily created on hot-dip Sn-coated copper utilizing custom-tailored DLIP and adjusting the frictional asymmetry, without significantly affecting the electrical behavior. One analogy for this anisotropy is the 'mechanical diode' phenomenon. However, these results are not generic, as they are obtained through very unique testing settings. Future work will address a broader range of loads, connection speeds and counter-body geometries.

Supplementary Information The online version contains supplementary material available at https://doi.org/10.1007/s11249-023-01799-0.

Acknowledgements The authors gratefully acknowledge funding in the ZuMat project, supported by the State of Saarland from the European Regional Development Fund (Europäischen Fonds für Regionale Entwicklung, EFRE).

Author contributions Silas Schütz: Investigation, Formal analysis, Data curation, Writing – original draft. Sebastian Suarez: Conceptualization, Methodology, Formal analysis, Funding acquisition, Writing – Review & Editing. Frank Mücklich: Supervision, Resources, Funding acquisition, Writing – Review & Editing.

Funding Open Access funding enabled and organized by Projekt DEAL. This study was supported by European Regional Development Fund

Data Availability Data will be made available on request.

Declarations

Competing Interests The authors declare that they have no known competing financial interests or personal relationships that could have appeared to influence the work reported in this paper.

References

1. Ma, S., et al.: Bioinspired 3D printed locomotion devices based on anisotropic friction. Small **15**(1), 1–13 (2019). https://doi.org/10.1002/smll.201802931
2. Hazel, J., Stone, M., Grace, M., Tsukruk, V.: "Nanoscale design of snake skin for reptation locomotions via friction anisotropy. J. Biomech. **32**(5), 477–484. https://doi.org/10.1016/S0021-9290(99)00013-5
3. Tramsen, H.T., Gorb, S.N., Zhang, H., Manoonpong, P., Dai, Z., Heepe, L.: Inversion of friction anisotropy in a bioinspired asymmetrically structured surface". J. R. Soc. Interface (2018). https://doi.org/10.1098/rsif.2017.0629
4. Schütz, S., Suarez, S., Britz, D., Mücklich, F.: Generation of asymmetric topographic structures in Cu-Sn connectors using extended direct laser interference patterning for the tailoring of insertion and removal forces in Proc. IEEE 67th Holm Conference on Electrical Contacts, 2022, pp. 240–246
5. Zentralverband Elektrotechnik- und Elektronikindustrie - ZVEI Ev: Ausfallraten für Bordnetz- Komponenten im Automobil. Erwartungswerte und Bedingungen. Cologne, Germany, 2021
6. Endres, H. (ed.): Praxishandbuch Steckverbinder, 2nd edn. Kindle ebooks, Seattle (2012)
7. Deng, X., Chawla, N., Chawla, K.K., Koopman, M.: Deformation behavior of (Cu, Ag)-Sn intermetallics by nanoindentation. Acta Mater. **52**(14), 4291–4303 (2004). https://doi.org/10.1016/j.actamat.2004.05.046
8. Daniel, C., Mücklich, F., Liu, Z.: Periodical micro-nano-structuring of metallic surfaces by interfering laser beams. Appl. Surf. Sci. **208–209**, 317–321 (2003). https://doi.org/10.1016/S0169-4332(02)01381-8
9. Bieda, M., Siebold, M., Lasagni, A.F.: Fabrication of sub-micron surface structures on copper, stainless steel and titanium using picosecond laser interference patterning. Appl. Surf. Sci. **387**, 175–182 (2016). https://doi.org/10.1016/j.apsusc.2016.06.100
10. Müller, D.W., Fox, T., Grützmacher, P.G., Suarez, S., Mücklich, F.: Applying ultrashort pulsed direct laser interference patterning for functional surfaces. Sci. Rep. (2020). https://doi.org/10.1038/s41598-020-60592-4
11. Gachot, C., et al.: Dry friction between laser-patterned surfaces: role of alignment, structural wavelength and surface chemistry. Tribol. Lett. **49**(1), 193–202 (2013). https://doi.org/10.1007/s11249-012-0057-y
12. Gachot, C., Rosenkranz, A., Hsu, S.M., Costa, H.L.: A critical assessment of surface texturing for friction and wear improvement. Wear **372–373**, 21–41 (2017). https://doi.org/10.1016/j.wear.2016.11.020
13. Grützmacher, P.G., Profito, F.J., Rosenkranz, A.: Multi-scale surface texturing in tribology-current knowledge and future perspectives. Lubricants (2019). https://doi.org/10.3390/lubricants7110095
14. Scharf, T.W., Prasad, S.V.: Solid lubricants: a review. J. Mater. Sci. **48**(2), 511–531 (2013). https://doi.org/10.1007/s10853-012-7038-2
15. Voisiat, B., Alamri, S., Lasagni, A.F.: One-step fabrication of asymmetric saw-tooth-like surface structures on stainless steel using direct laser interference patterning. Mater. Lett. **245**, 183–187 (2019). https://doi.org/10.1016/j.matlet.2019.03.007
16. Alamri, S., El-Khoury, M., Aguilar-Morales, A.I., Storm, S., Kunze, T., Lasagni, A.F.: Fabrication of inclined non-symmetrical periodic micro-structures using direct laser interference patterning. Sci. Rep. **9**(1), 1–12 (2019). https://doi.org/10.1038/s41598-019-41902-x
17. So, A.C.K., Chan, Y.C.: Aging studies of Cu-Sn intermetallic compounds in annealed surface mount solder joints. In Proceedings 46th Electronic Components and Technology Conference, Orlando, FL, USA, 1996, pp. 1164–1171. doi: https://doi.org/10.1109/ECTC.1996.550884.
18. Lide, D.R.: CRC handbook of chemistry and physics. CRC Press, Boca Raton (2010)
19. Frederikse, H.P.R., Fields, R.J., Feldman, A.: Thermal and electrical properties of copper-tin and nickel-tin intermetallics. J. Appl. Phys. **72**(1), 2879–2882 (1992). https://doi.org/10.1063/1.351487
20. Mücklich, F., Lasagni, A., Daniel, C.: Laser Interference Metallurgy – using interference as a tool for micro/nano structuring. Z. Met. **97**(10), 1337–1344 (2006)
21. Lasagni, A., D'Alessandria, M., Giovanelli, R., Mücklich, F.: Advanced design of periodical architectures in bulk metals by means of laser interference metallurgy. Appl. Surf. Sci. **254**(4), 930–936 (2007). https://doi.org/10.1016/j.apsusc.2007.08.010
22. Lasagni, A.F., Roch, T., Langheinrich, D., Bieda, M., Wetzig, A.: Large area direct fabrication of periodic arrays using interference patterning. Phys. Procedia **12**, 214–220 (2011). https://doi.org/10.1016/j.phpro.2011.03.125
23. Alderete, B., Puyol, R., Slawik, S., Espin, E., Mücklich, F., Suarez, S.: Multipurpose setup used to characterize tribo-electrical properties of electrical contact materials. MethodsX **8**, 101498 (2021). https://doi.org/10.1016/j.mex.2021.101498
24. Buresch, I: Möglichkeiten der Eigenschaftsoptimierung von Zinnoberflächen für Steckkontakte," in VDE Fachberichte: Kontaktverhalten und Schalten - 22. Fachtagung Albert-Keil-Kontaktseminar. 2013. https://www.vde-verlag.de/proceedings-en/453530016.html
25. Kaiser, V: Technischer Leitfaden-TLF 0214 Validierung von Automotive-Niedervolt-Steckverbindern. Frankfurt am Main. 2021. www.zvei.org

26. Holm, R.: Electric contacts, theory and applications, 4th edn. Springer-Verlag, Berlin (2000)